An Investigation on the Effect of Magnetic Field on Induced Fluid Flow and Heat Transfer Using CFD-DEM

Abstract

Magnetic nanofluids are smart materials that have gained significant attention recently due to their unique properties and potential applications in various fields. These fluids consist of magnetic nanoparticles dispersed in a carrier fluid, which an external magnetic field can manipulate. A magnetic field causes particles to aggregate in chain-like formations, enhancing their conduction heat flux. This Anisotropic phenomenon has been extensively researched in the literature. This study has also investigated the convection heat flux that arises from the induced fluid flow resulting from particle motion. A numerical simulation was performed using CFD-DEM coupling modeling through COMSOL Multiphysics 6.1. The findings indicate that as the magnetic field strength increases, the chain-like clusters in the magnetic fluid become more prominent, thereby enhancing the anisotropic nature of conduction heat transfer in the fluids. A higher conduction heat flux is observed in magnetic fields parallel to the temperature gradient compared to perpendicular ones. Furthermore, the particles' motion disrupted the base fluid's hydrodynamic and thermal boundary layer. No convection heat transfer was detected in magnetic fields of 0.01, 0.02, and 0.05 Tesla. However, at 0.1 Tesla and a 4% volume concentration, a significant disparity between total and conduction heat transfer was observed, suggesting the presence of convection heat transfer.

Keywords: Magnetic nanofluid, Anisotropic heat transfer, Induced fluid flow, Convection heat transfer, Two way coupling, CFD-DEM.

Accepted Manuscript

1. Introduction

Magnetic nanofluids are nonmagnetic base fluids containing magnetic nanoparticles, such as iron or its oxide, like magnetite (Fe_3O_4).These particles typically range in size from 1 to 100 nm. To keep the nanoparticles suspended in the system, chemical and physical methods can be used. Examples of these methods include adding surfactants such as oleic acid and using an ultrasonic device [1]. Magnetic nanofluids have the advantage of combining the flowability of the base fluid with the thermal conductivity of solid particles. An external field, such as a magnet, can manipulate magnetic particles, allowing them to act like a smart fluid. In addition to issues concerning heat transfer, magnetic nanofluids have a wide range of uses in various areas, including medicine, biology, electronics, and mechanical engineering. This is due to their adjustable characteristics, making them versatile [2]. Notably, research on the heat transfer characteristics of magnetic nanofluids is generally classified into two main categories: conduction and convection.

Many studies have shown that thermal conductivity increases when the magnetic field is aligned with the temperature gradient [3-9]. This creates a chain-like structure along the temperature gradient, facilitating more efficient heat transfer. This characteristic is known as anisotropy due to its dependence on the direction [10]. This phenomenon has also proved in this research.

Furthermore, the convection heat transfers of magnetic nanofluids were also considered [11]. Volker et al. [12] and Engler et al. [13] studied natural convection experimentally. They found that when the magnetic nanofluid is simultaneously subjected to a magnetic field and a temperature gradient, there is a net driving force called thermomagnetic convection. In order to better understand thermomagnetic convection, it is important to consider a specific type of magnetic nanofluid that is temperature-sensitive, with magnetization increasing as the temperature decreases. In such fluids, the magnetization near the cold wall is higher than that near the hot wall. According to Fig. 1, the particles near the wall at temperature T_2 become more magnetized and move more rapidly toward the wall at temperature T_1 ($T_1 > T_2$), following the direction of the external magnetic field (H) which enhance natural convection. Therefore, the Rayleigh number (Ra) is obtained as below [14]:

$$Ra = Ra_T + Ra_m \tag{1}$$

where Ra_T and Ra_m represent thermogravitational Rayleigh number and magnetic Rayleigh number, respectively.

Accepted Manuscript

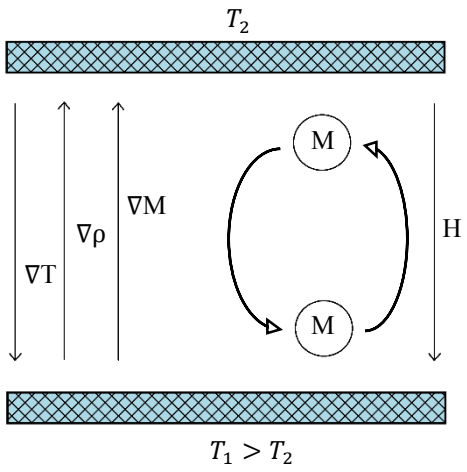

Fig. 1. Schematic representation of the principle behind the situation in which thermomagnetic and natural convection exist.

On the other hand, Goharkhah et al. [15] studied experimentally forced convection of magnetite ferrofluid in a heated tube under the influence of constant and alternating magnetic field. The heat transfer enhancement is increased significantly up to 18.9% and 31.4% by application of constant and alternating magnetic field, respectively.

In this study, we do not investigate the effect of temperature on particle magnetization; instead, we focus directly on the influence of particle motion on the base fluid. In addition, to achieve a more precise and accurate analysis of convection heat transfer, by setting the initial velocity of the base fluid close to zero, we examine the impact of particle motion on fluid velocity disturbances. These distinctions highlight how this study differs from prior research on thermomagnetic and forced convection phenomena. A key aspect of this work is to illustrate how particle movement influences induced fluid flow and ultimately the convection heat transfer. To achieve this goal, a two-way coupling model was implemented using CFD-DEM, where the base fluid and the particles are treated as continuous and discrete phases. The novelty of this research lies in understanding and visualizing the influence of subtle nanoparticle movements on fluid layers and thermal convection.

Accepted Manuscript

2. Modeling

2.1 Geometry

A two-dimensional channel with a length of 300 nm has been studied. Two constant temperature boundary conditions are considered at the top and bottom, indicating the hot and cold regions, respectively ($T_h = T_c + 10^{-11}\ K$). To observe the effect of particle movement on the fluid, the fluid velocity should be as low as possible. Therefore, the average inlet velocity is $10^{-20}\ m/s$ and is also assumed fully developed. The outlet relative pressure is set to zero (Fig. 2).

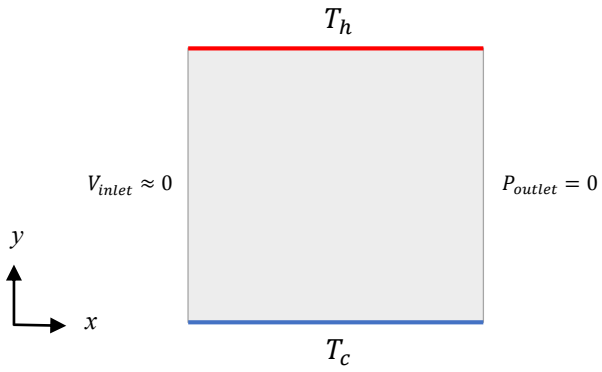

Fig. 2. Geometry and boundary conditions.

Once the system has reached thermally developed condition, 30 nm diameter spherical particles (Fe_3O_4) are randomly dispersed in the base fluid (water). The parameters used for this study are outlined in Table 1. The two-dimensional volume fraction is calculated as the ratio of the area occupied by particles to the total simulation area. In this study, three-dimensional volume fraction was calculated based on two-dimensional volume fraction according to the following relation proposed by Hoomans et al. [16, 17]. This is because the volume fraction calculated in this manner is based on a two-dimensional analysis, which is inconsistent with the empirical correlations used to calculate the drag force acting on a particle that are derived from actual three-dimensional systems. To correct for this inconsistency, the area-based volume fraction (φ_{2D}) was converted to a three-dimensional volume fraction (φ_{3D}) using the following equation.

$$\varphi_{3D} = \frac{2}{\sqrt{\pi\sqrt{3}}} {\varphi_{2D}}^{3/2} \tag{2}$$

Table 1
Important parameters used in this study.

parameter	symbol	value	unit
Temperature of the particle and the base fluid	T	293.15	K
Vacuum magnetic permeability	μ_0	$4\pi \times 10^{-7}$	N/A^2
Fluid viscosity	μ	0.000891	$kg/m\,.s$
Fluid density	ρ_f	0.998	g/cm^3
Particle density	ρ_p	5.15	g/cm^3
Fluid thermal conductivity coefficient	k_f	0.6	$W/m\,.K$
Particle thermal conductivity coefficient	k_p	3.8	$W/m\,.K$

Accepted Manuscript

2.2 Fluid phase governing equations

The base fluid is the continuous phase and its governing equations are the continuity and Navier-Stokes equations.

$$\frac{\partial(\rho_f \varphi_{3D})}{\partial t} + \boldsymbol{\nabla}.\left(\rho_f \varphi_{3D} \boldsymbol{u}\right) = 0 \tag{3}$$

$$\rho_f \left(\frac{\partial(\varphi_{3D}\boldsymbol{u})}{\partial t} + (\varphi_{3D}\boldsymbol{u}.\boldsymbol{\nabla})\boldsymbol{u}\right) = -\varphi_{3D}\nabla p + \mu\nabla^2(\varphi_{3D}\boldsymbol{u}) + \boldsymbol{F}^{f-p} \quad (4)$$

where $t, \rho_f, \varphi_{3D}, \boldsymbol{u}$, are time, fluid density, 3D volume fraction and fluid velocity vector, respectively. p is fluid pressure and $\boldsymbol{F}^{f-p}$ represents volumetric fluid–particle interaction force.

2.3 Equations of particle motion

Particles are tracked individually and treated as a discrete phase. They have two types of translational and rotational motion defined by linear momentum (Newton's second law of motion) and angular momentum, respectively.

2.3.1. Linear momentum

Translational motion is the movement of particles concerning a fixed origin of coordinates. This type of motion is caused by forces acting upon the particles, causing them to move in a specific direction. Therefore, the resultant force determines the position of the particle ($\boldsymbol{r}_i$) in the subsequent time step. Where $\boldsymbol{g}, m_i, \boldsymbol{v}_i$ are the ith-particle's gravity, mass, and linear velocity.

$$\boldsymbol{F}_i^{Magnetic} + \boldsymbol{F}_i^{Dipole} + \boldsymbol{F}_i^{Contact} + \boldsymbol{F}_i^{Drag} + m_i\,\boldsymbol{g} = m_i\frac{d\boldsymbol{v}_i}{dt} = m_i\frac{d^2\boldsymbol{r}_i}{dt^2} \quad (5)$$

2.3.1.1. External magnetic force

In this research, the external magnetic field is uniform, thus resulting in a zero value for the force. Put it another way, the external field does not cause translational motion of particles [18].

$$\boldsymbol{F}_i^{Magnetic} = \mu_0(\boldsymbol{M_i}.\nabla)\boldsymbol{H} \quad (6)$$

2.3.1.2. Magnetic dipole force

As well as the external field, each nanoparticle has a magnetic field affecting its neighbors. $\boldsymbol{F}_{ij}^{Dipole}$ is the force that jth-nanoparticle exerts on the ith-nanoparticle. It is directly proportional to the magnetic moment of the particles ($\boldsymbol{M}_i$) and inversely proportional to the distance between particles ($\boldsymbol{r}_{ij}$).

$$\boldsymbol{F}_{ij}^{Dipole} = \frac{3\mu_0}{4\pi|\boldsymbol{r}_{ij}|^5}\left[(\boldsymbol{M}_i.\boldsymbol{r}_{ij})\boldsymbol{M}_j + (\boldsymbol{M}_j.\boldsymbol{r}_{ij})\boldsymbol{M}_i + (\boldsymbol{M}_i.\boldsymbol{M}_j)\boldsymbol{r}_{ij} - 5\frac{(\boldsymbol{M}_i.\boldsymbol{r}_{ij})(\boldsymbol{M}_j.\boldsymbol{r}_{ij})}{|\boldsymbol{r}_{ij}|^2}\boldsymbol{r}_{ij}\right] \quad (7)$$

$$\boldsymbol{r}_{ij} = \boldsymbol{r}_j - \boldsymbol{r}_i \quad (8)$$

The external magnetic field affects the direction and magnitude of the magnetic moment vector (magnetization). It attempts to align the magnetic moment of the particles with itself. As

Accepted Manuscript

the field strength increases, the particle magnetization increases and finally reaches a saturation value [19].

Table 2
Magnetization of spherical magnetite particles with a diameter of 30 nm under magnetic fields with different strengths [19].

Magnetic field intensity (T)	0	0.01	0.02	0.05	0.1	0.2	0.5	1
Magnetization (emu/g)	1.2	9	19	34	41	46	52	54

2.3.1.3 Contact force

Particles behave like soft spheres, forming an overlap after the collision. The contact force calculated based on linear spring-dashpot collision concepts proposed by Cundall and Strack [20].

$$\boldsymbol{F_{ij}}^{Contact} = (K\delta + \gamma(\boldsymbol{V}_{ij}.\boldsymbol{e}_{ij}))\,\boldsymbol{e}_{ij} \quad (9)$$

$$\boldsymbol{V}_{ij} = \boldsymbol{V}_j - \boldsymbol{V}_i \quad (10)$$

$$\boldsymbol{e_{ij}} = \frac{\boldsymbol{r_{ij}}}{|\boldsymbol{r_{ij}}|} \quad (11)$$

It contains the spring stiffness constant K, damping term γ, and δ, the overlap value. $\boldsymbol{V}_{ij}, \boldsymbol{e_{ij}}$ are the relative velocities of two adjacent particles and normalized vector of distance between particles.

We can estimate the value of the spring constant and damping term using the following equation as the Ansys Fluent guide 2020 R2 suggests:

$$K = \frac{\rho_p d_p \pi\,|v_{ij}|^2}{3\,\varepsilon_D{}^2} \quad (12)$$

$$\gamma = \frac{-m_p \ln\eta}{t_{collision}} \quad (13)$$

$$t_{collision} = \sqrt{(\pi^2 + \ln^2\eta)\frac{m_p}{2K}} \quad (14)$$

Where ρ_p, d_p, m_p are particle density, particle diameter and particle mass. ε_D is the fraction of the diameter for allowable overlap ($\frac{\delta}{d_p}$). η is the coefficient of restitution for the dashpot term and $0 < \eta \leq 1$.

2.3.1.4. Drag force

The force applied against the particle from the fluid is called drag force. The base fluid is a Newtonian fluid and the flow remains laminar ($Re \ll 1$), so Stokes equation has been used [21]. $\boldsymbol{U}$ and $\boldsymbol{V}$ indicate the fluid and particle velocity vector, respectively.

$$\boldsymbol{F}_i{}^{Drag} = \frac{18\,\mu}{\rho_p\, d_p^2} m_p(\boldsymbol{U} - \boldsymbol{V}) \quad (15)$$

Accepted Manuscript

2.3.2. Angular momentum

Rotational motion is the movement of particles relative to their center, which is caused by the torque acting on them. Therefore, the resultant torque determines the angular position of the particle ($\boldsymbol{\theta}_i$) in the next time step [22].

$$\boldsymbol{T}_i^{Field} - \xi_r \boldsymbol{\omega}_i = I_i \frac{d\boldsymbol{\omega}_i}{dt} = I_i \frac{d^2\boldsymbol{\theta}_i}{dt^2} \quad (16)$$

Where $\boldsymbol{T}_i^{Field}, \xi_r, \boldsymbol{\omega}_i, I_i$ are external magnetic moment, rotational drag force coefficient, angular velocity and moment of inertia, respectively.

$$\boldsymbol{T}_i^{Field} = \boldsymbol{M}_i \times \boldsymbol{H} \quad (17)$$

$$\xi_r = \pi d_p^3 \mu \quad (18)$$

$$I_i = m_i \frac{d_p^2}{10} \quad (19)$$

2.4. Thermal equation

The equation of heat transfer in Cartesian coordinates containing fluid is as follows [21].

$$\rho_f C_p \left(\frac{\partial T}{\partial t} + \boldsymbol{u} . \nabla T\right) + \nabla . (-k_{cell} \nabla T) = 0 \quad (20)$$

Where C_p, T, k_{cell} are the specific heat capacity at constant pressure, absolute temperature and thermal conductivity coefficient of the cell. The thermal conductivity coefficient of a cell is determined by the material occupying it. The values of 0.6 and 3.8 W/m.K are regarded as the respective properties of fluid and particle. By default, in COMSOL Multiphysics 6.1, k_{cell} equals to k_f (0.6 W/m.K). Thus, for regions containing particles, a UDF code was written to correct k_{cell} to reach k_p (3.8 W/m.K). For regions containing both particles and fluid, the thermal conductivity is determined based on an average value.

2.5. Simulation details

2.5.1. Heat transfer coefficient

As seen in Fig. 2, the temperature gradient is aligned with the y-axis. Therefore, the heat flux is computed in this direction, containing conduction and convection.

$$q_{total}|_y = q_{conduction}|_y + q_{convection}|_y \quad (21)$$

$$k_{eff} = \frac{q_{total}|_y}{\partial T/\partial y} = \frac{q_{conduction}|_y}{\partial T/\partial y} + \frac{q_{convection}|_y}{\partial T/\partial y} = k + f(h) \quad (22)$$

Where k is the thermal conductivity of the system and $f(h)$ indicates the convective heat transfer coefficient, computed using Fourier's law. k is attributed to particle chaining and has been

Accepted Manuscript

extensively studied in the literature, but $f(h)$ is a novel concept and arises from induced fluid flow. To compute k, a one-way coupling modeling approach was employed to avoid any induced fluid flow. In contrast, $f(h)$ requires a two-way coupling modeling approach with a constant thermal conductivity coefficient of 0.6 W/m.K for the cell to avoid any chain-like effects. Ultimately, $f(h)$ is obtained by deducting the thermal conductivity contribution of water from the heat flux.

2.5.2. Cut-off radius

$\boldsymbol{F}_{ij}{}^{Dipole}$ is influenced by the presence of other particles. However, as the strength of this force diminishes significantly with increasing distance ($\boldsymbol{F}_{ij}{}^{Dipole} \sim \frac{1}{|\boldsymbol{r}_{ij}|^5}$), it is possible to limit its application within a specific range to reduce computation time. This range is defined as the cut-off radius, which is set at 2.5 times the diameter of the particles [23]. Beyond this radius, the magnetic dipole force between particles is considered zero (as shown in Fig. 3). The UDF code is executed from 70 microseconds onwards.

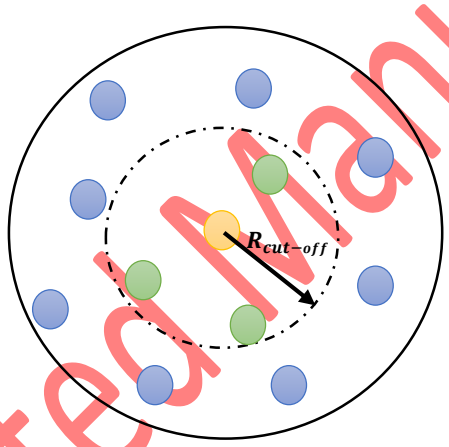

Fig. 3. The cut-off radius of a magnetic particle [23].

3. Results and discussion

The results of this study cover three aspects, organized as follows. The trajectory of magnetic particles as well as a discussion about macro- and micro-scale phenomenon in the chaining process are presented first, following by a discussion about the induced flow during the chaining process. This section ends with a detail discussion about the thermal effect of induced flow during the chaining of magnetic nanoparticles.

3.1. Particle motion and chaining Process

Simulation was carried out for detecting the chaining of nanoparticles according to the conditions explained in modeling section. The snapshots of the nanoparticles' position, velocity, and magnetic moment vector (Arrow) are illustrated in Fig. 4. The spheres and arrows are colored

Accepted Manuscript

according to the magnitude of translational and angular velocity, which is attributed to the dipole force (Eq. 7) and external torque (Eq. 17), respectively. Nanoparticles are dispersed inside the domain randomly at zero time. As can be seen in this figure, the dispersed nanoparticles in fluid condition is gradually transformed in to a chaining ones by elapsing time. At early stage of this process (i.e., t= 0.1 μs), the nanoparticles moves and rotate because of dipole and external magnetic forces. The translational and angular velocity of nanoparticles are low and the arrows of angular velocity are in various directions. After elapsing 1 μs of the process, when the particles move towards each other and the distance between the nanoparticles becomes less, the translational velocity increases. However, the contact force (Eq. 9) prevents two particles from overlapping completely. The angular velocity increases until the particles align with the external magnetic field (2 μs). Consequently when particles reach each other, the translational velocity of the particles decreases considerably and they formed chain like structures. In this situation, the contact force compensate the dipole force. By forming this primer chains, the movement of particles in chain becomes more restricted and in return the chain like structures grow. Finally, at 100 μs, no motion of particles is observed, suggesting that the magnetic nanofluid had achieved stability. Nanoparticles are shaped in a chain along the y-axis due to the influence of the magnetic field, resulting in the anisotropic properties.

Accepted Manuscript

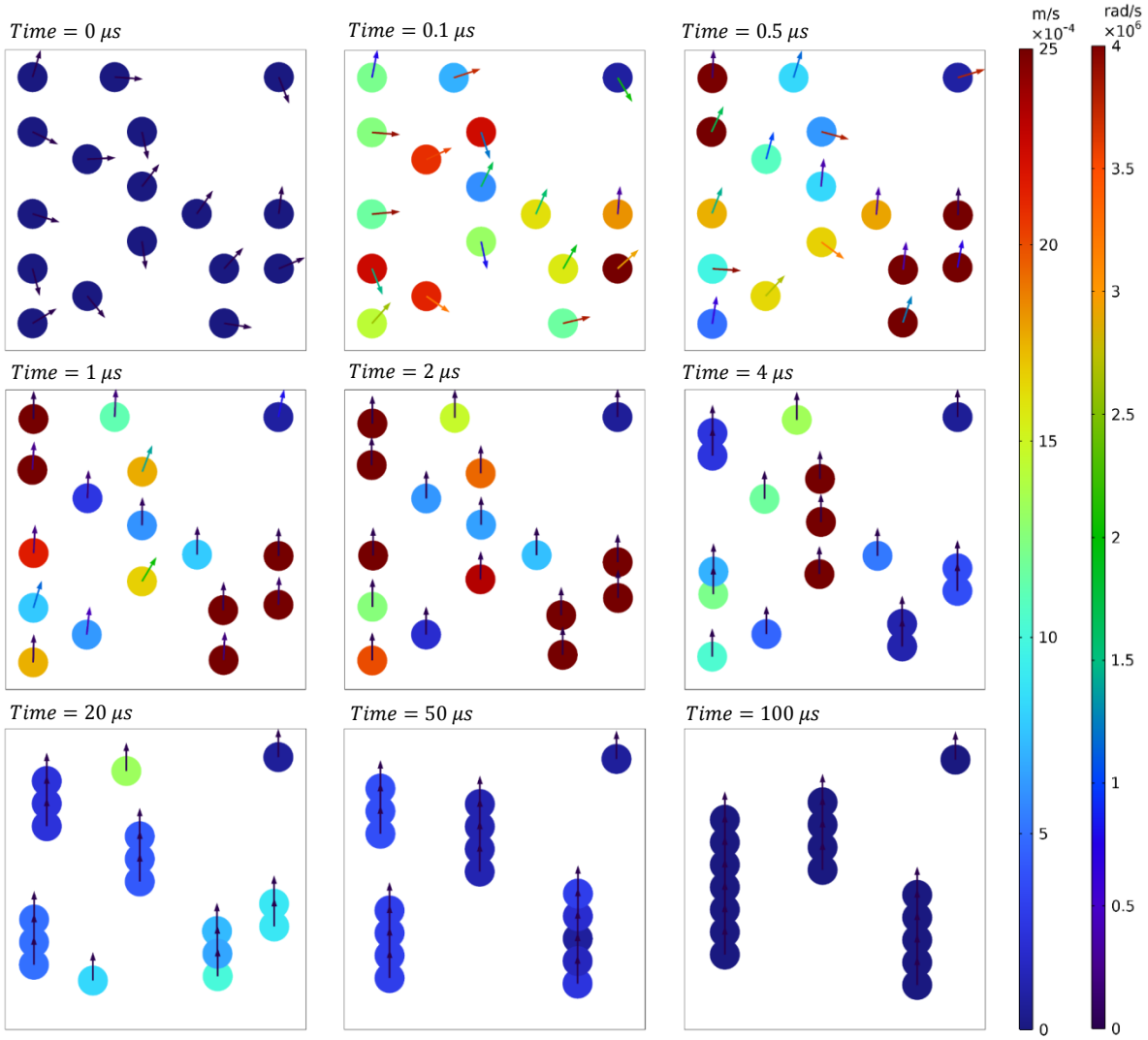

Fig. 4. Position, translational velocity (m/s), and angular velocity (rad/s) of the particles in a magnetic nanofluid containing 4% volume fraction nanoparticle under a magnetic field of 0.1 Tesla over time.

Acce

3.2. Induced fluid flow

The movement of particles in the domain leads to fluid flow and disturbance in the hydrodynamic boundary layer. As the induced fluid velocity can vary significantly, the results are divided into three stages: initial, intermediate, and final.

3.2.1. Initial time

Fig. 5 illustrates the induced fluid velocity at the initial times in picoseconds. The legend values are based on the input velocity of the base fluid. It is evident that after 1 ps, the fluid is disturbed, which is much more sensitive than the particle, needing a more minor time step. At 10 ps, the picture turns almost red, indicating that a legend with a more significant order should be used.

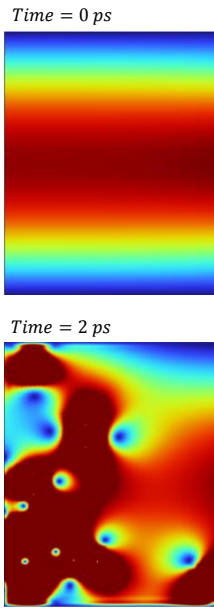

Fig. 5. Induced fluid velocity at initial time in a magnetic nanofluid containing 4% volume fraction nanoparticle under a magnetic field of 0.1 Tesla over time.

3.2.2. Intermediate time

Fig. 6 demonstrates the induced fluid velocity at the intermediate times in microseconds with a legend in order of $10^{-11}\,m/s$. For better description of the process, the snapshots of the spatial velocity distribution of particles, in the same bed described in Fig. 4, are shown in Fig. 6. An increase in particle speed leads to a corresponding rise in fluid velocity. This phenomenon is displayed in moments of 1 and 2 microseconds. As can be seen in this figure, the induced flows are gradually disappeared by decreasing the translational and rotation movement of particles and chain like structure formation.

Accepted Manuscript

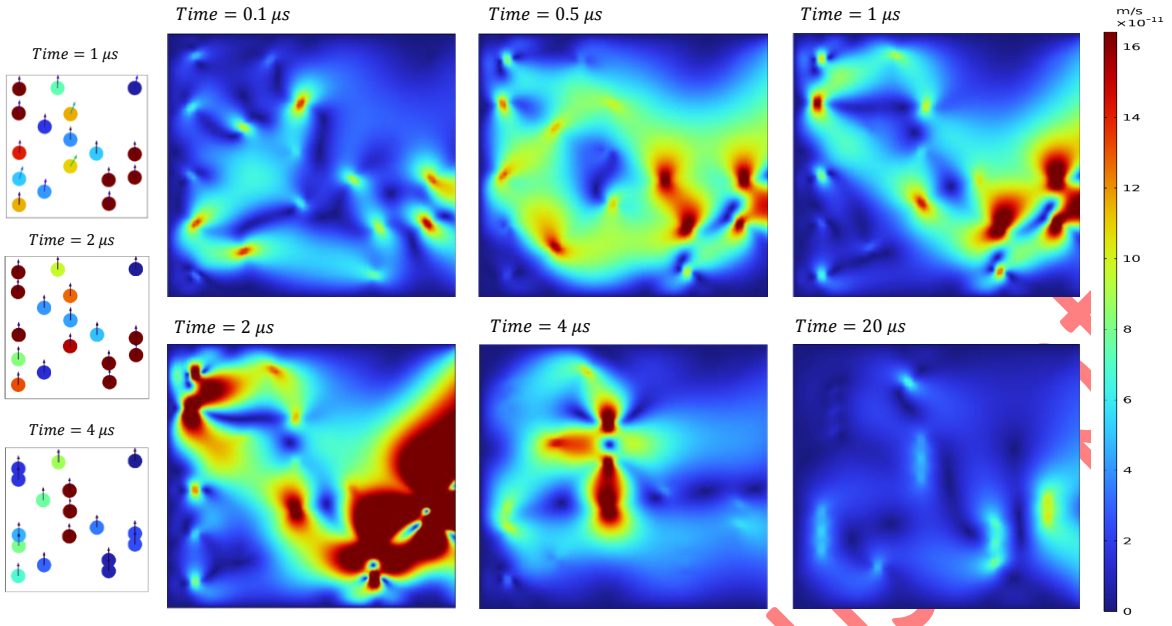

Fig. 6. Induced fluid velocity at intermediate time in a magnetic nanofluid containing 4% volume fraction nanoparticle under a magnetic field of 0.1 Tesla over time.

3.2.3. Final time

The induced fluid velocity decreases during the stability of the magnetic nanofluid. As the distance between particles or chains increases (beyond 100 microseconds), the dipole force decreases, and they no longer affect one another. Meanwhile, the external magnetic field is constant and doesn't cause any translational motion. This combination of factors stabilizes the magnetic nanofluid and returns to its initial velocity boundary layer state (Fig. 7).

Accepted Manuscript

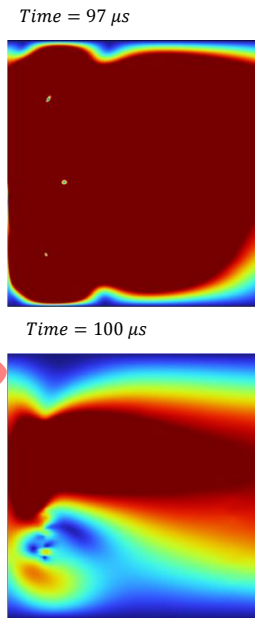

Fig. 7. Induced fluid velocity at final time in a magnetic nanofluid containing 4% volume fraction nanoparticle under a magnetic field of 0.1 Tesla over time.

3.3. Thermal behavior of magnetic nanofluid

3.3.1. Temperature gradient

The particles in a fluid can cause disturbances in the thermal boundary layer due to their different thermal conductivity and induced fluid flow. This phenomenon is illustrated in Fig. 8, which depicts the dimensionless temperature contour of the base fluid with and without particles. In the absence of particles, the temperature distribution is determined by the distance from the hot and cold walls. However, the layer is disrupted in the presence of particles, leading to an altered boundary layer structure. Nanoparticles have higher thermal conductivity than the base fluid (3.8 to 0.6 w/m.K) and a magnetic field enables them to enhance heat transfer by bridging hot and cold zones. The dimensionless temperature of the fluid is defined as follows.

$$\theta = \frac{T - T_c}{T_H - T_c} \tag{23}$$

Accepted Manuscript

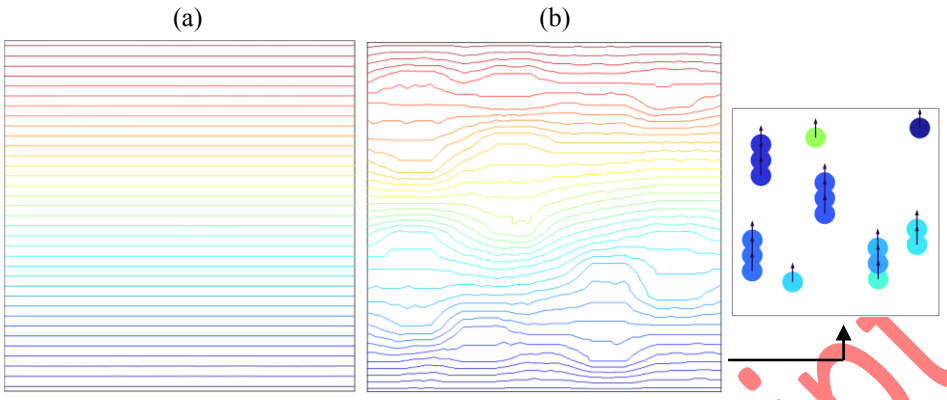

Fig. 8. Dimensionless temperature contour of the base fluid (a) without and (b) with particles in a magnetic nanofluid containing 4% volume fraction nanoparticle under a magnetic field of 0.1 Tesla at $t = 20\ \mu s$.

3.3.2. Conduction heat transfer (k)

3.3.2.1. Thermal conductivity in the absence of a magnetic field

Fig. 9 illustrates the ratio of magnetic nanofluid thermal conductivity coefficient (k) to base fluid (k_f) at various concentrations without a magnetic field. The diagram presents results from experimental research conducted by Zhu et al. [24] and Abareshi et al. [25], as well as computational modeling performed in this study and classical models such as Maxwell and Jeffrey models. According to Fig. 9, classical models are not suitable for predicting thermal conductivity of nanoparticles. The diameter of the particles in Zhu et al. experiment was 10 nm, while present work used 30 nm particles. In the study by Abareshi et al. [25], cubic-shaped nanoparticles ranging in size from 15 to 22 nanometers were used. These variations in particle size and shape contributed to the differences observed in the values presented in the graph. Overall, increasing the concentration leads to an increase in the thermal conductivity coefficient in nanofluid.

Accepted Manuscript

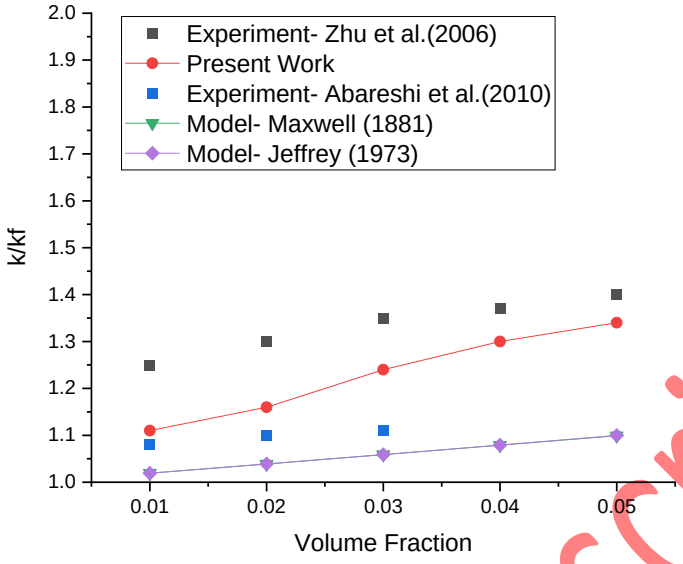

Fig. 9. The ratio of thermal conductivity coefficient of magnetic nanofluid to base fluid (water) at various concentrations without a magnetic field.

3.3.2.2. Thermal conductivity under a parallel magnetic field

Fig. 10 shows how the system's thermal conductivity coefficient to the base fluid (k/k_f) grows over time. The increase is evident in chain formation, particularly at higher volume fractions. Anisotropic properties formed by magnetic nanoparticles act as solid bridges. This phenomenon has been observed many times in the literature [4, 5, 26, 27].

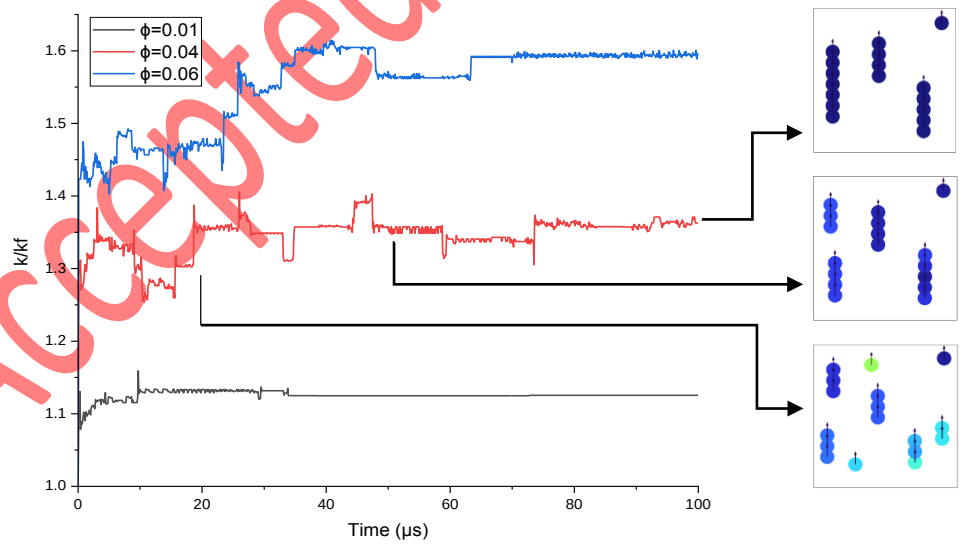

Fig. 10. The ratio of thermal conductivity coefficient of magnetic nanofluid to base fluid (water) at 0.1 T in the presence of parallel magnetic field.

Accepted Manuscript

3.3.2.3. Thermal conductivity under a perpendicular magnetic field

Fig. 11 illustrates thermal conductivity under 1 Tesla magnetic field in parallel and perpendicular directions to the temperature gradient. The concentration increase enhances thermal conductivity in both directions, with a more pronounced effect when aligned with the magnetic field. The anisotropic structure resulting from chain formation, as shown in Fig. 4, suggests anticipated variations in thermal behavior based on alignment with or perpendicular to the magnetic field direction.

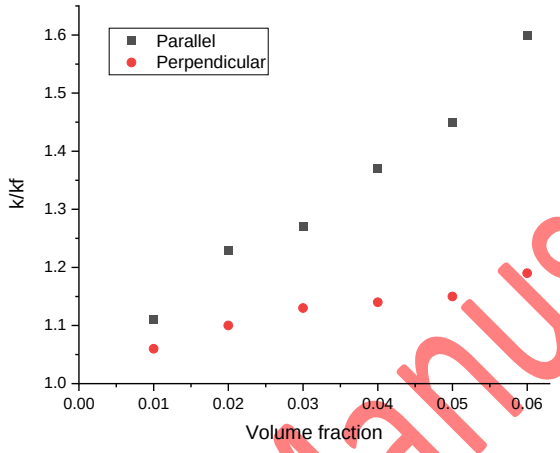

Fig. 11. The thermal conductivity ratio in magnetic nanofluid to water under 1 Tesla magnetic field at different volume fractions in both parallel and perpendicular magnetic fields.

3.3.3. Convection heat transfer ($f(h)$)

In the absence of magnetic field and even magnetic fields of 0.01, 0.02 and 0.05 Tesla, no remarkable convection heat transfer was observed (Fig. 12). It means the induced fluid flow in these intensities cannot increase the convection coefficient and therefore $f(h) \approx 0$ (Eq.22).

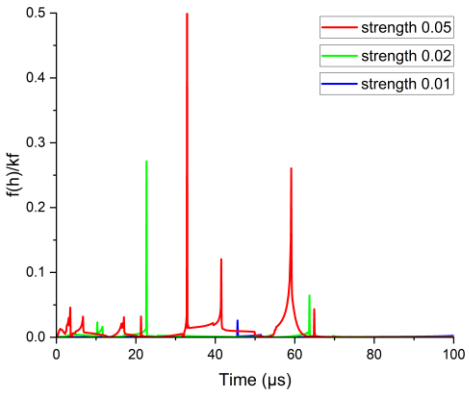

Fig. 12. The ratio of convection heat transfer coefficient in a magnetic nanofluid containing 4% volume fraction nanoparticle under a magnetic field of 0.01, 0.02 and 0.05 Tesla to base fluid thermal conductivity coefficient over time.

Accepted Manuscript

Fig. 13 shows convection heat transfer coefficient changes for a 4% volume fraction magnetic nanofluid under 0.1 Tesla field, compared to the base fluid thermal conductivity coefficient $(f(h)/k_f)$ over time. Particle movement causes induced fluid flow, leading to enhanced convection heat transfer. It demonstrates up to a 40% enhancement in thermal convection compared to pure water, whereas Ashjaee et al. [28] reported a 38% increase in convective heat transfer for a 3% volume fraction under a 0.12 Tesla magnetic field in laminar flow conditions. However, beyond 50 microseconds, chain movement lacks the speed needed to sustain induced fluid flow and further increase convection heat transfer.

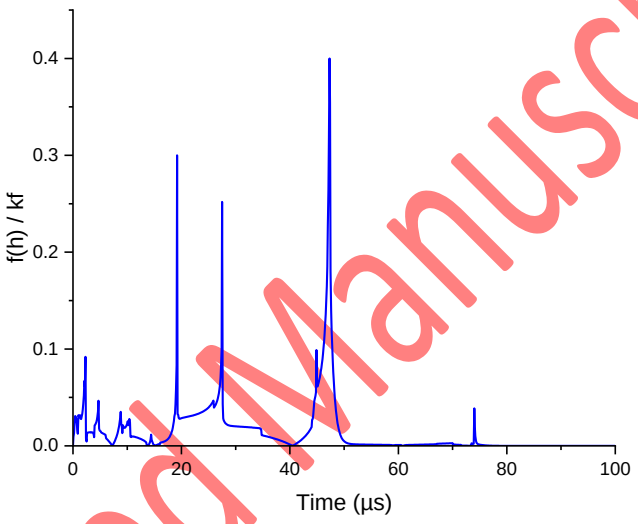

Fig. 13. The ratio of convection heat transfer coefficient in a magnetic nanofluid containing 4% volume fraction nanoparticle under a magnetic field of 0.1 Tesla to base fluid thermal conductivity coefficient over time.

3.4.2.3. Total heat transfer coefficient $(k_{eff} = k + f(h))$

As seen in Fig. 14 a gap exists between the k_{eff} and k graphs due to the presence of $f(h)$. This distinction is noticeable before the magnetic nanofluid achieves stability. However, starting at 50 microseconds, these two graphs coincide. As shown in Fig. 4, the formation of long particle chains indicates that the particles have nearly reached a stable state within the nanofluid and can no longer move freely or contribute to thermal convection.

Accepted Manuscript

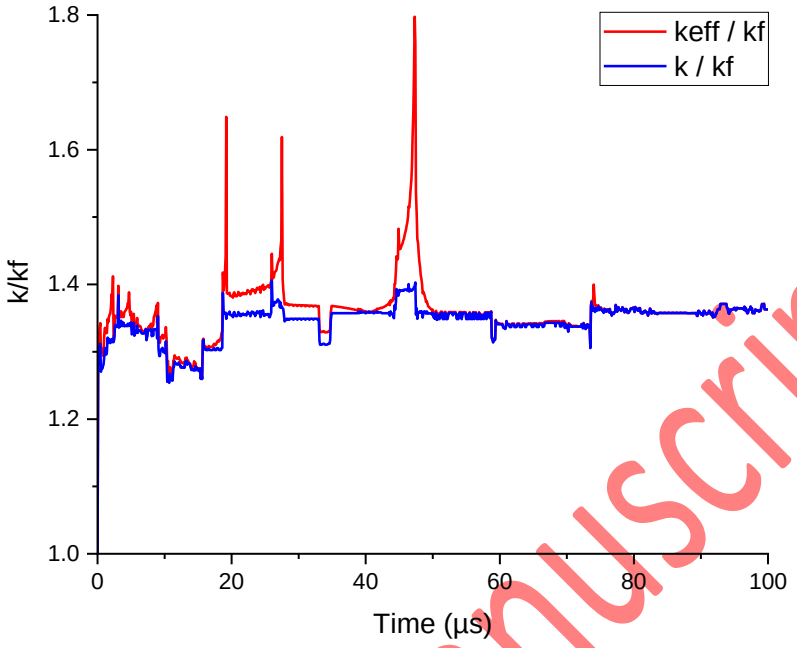

Fig. 14. Comparison of the total heat transfer coefficient (k_{eff}/k_f) and thermal conductivity (k/k_f) of a magnetic nanofluid under 0.1 Tesla field at a 4% volume fraction.

4. Conclusions

CFD-DEM method was used to investigate the induced fluid flow and thermal behavior of the magnetic nanofluid. Our findings can be summarized as follows:

- With an external magnetic field, particles exhibit translational and rotational motion, disrupting the fluid velocity profile. The fluid velocity is directly proportional to the particle velocity.
- Upon achieving stability in the magnetic nanofluid, the hydrodynamic boundary layer reverts to its initial state.
- The particle's thermal conductivity and induced fluid flow disrupt the fluid temperature profile.
- The model presented demonstrated superior prediction of thermal conductivity enhancement compared to the classical Maxwell and Jeffrey models In the absence of the magnetic field.
- Chaining of particles causes anisotropic properties and ultimately improves thermal conductivity along the temperature gradient.
- In magnetic fields with intensities of 0.01, 0.02, and 0.05 Tesla, the induced fluid flow is insufficient to enhance convective heat transfer. However, under 0.1 Tesla, a considerable gap is observed between thermal conductivity and total heat transfer, indicating the existence of convection heat transfer.

Accepted Manuscript

Nomenclature

T_h	hot wall of the channel (K)	T_c	cold wall of the channel (K)
φ	volume fraction (-)	ρ	density (kg/m^3)
μ	fluid viscosity $(kg/m.s)$	Re	Reynolds number
$\mathbf{u}$	fluid velocity (m/s)	$\mathbf{V}$	particle velocity (m/s)
μ_0	vacuum magnetic permeability (N/A^2)	$\mathbf{g}$	acceleration of gravity (m/s^2)
$\mathbf{M}_i$	magnetic moment of particle i $(A.m^2)$	$\mathbf{r}_i$	position of particle i (m)
$\mathbf{e}_{ij}$	unit vector position of particle i	$\mathbf{F_i}$	force on particle i (N)
$\mathbf{F}_i^{Drag}$	drag force on particle i (N)	$\mathbf{F_{ij}}^{Dipole}$	magnetic force on particle i from particle j (N)
$\mathbf{F}_i^{Magnetic}$	external magnetic force on particle i (N)	$\mathbf{F_{ij}}^{Contact}$	contact force on particle i from particle j (N)
$\mathbf{H}$	magnetic field (T)	K	spring constant (N/m)
γ	damping term $(N.s/m)$	δ	overlap value (m)
I_i	moment of inertia of particle i $(kg.m^2)$	$\boldsymbol{q}$	heat flux (W/m^2)
$\boldsymbol{\omega_i}$	angular velocity of particle i (rad/s)	k_{eff}	effective heat transfer coefficient $(W/m.K)$
$\boldsymbol{\theta_i}$	angular position of particle i (rad)	k	conduction hear transfer coefficient $(W/m.K)$
ξ_r	rotational drag coefficient of particle i $(kg.m^2/s)$	$f(h)$	convection hear transfer coefficient $(W/m.K)$
m_i	mass of particle i (kg)	$R_{cut-off}$	cut-off radius (m)
d_p	particle diameter (m)	t	time (s)
$\mathbf{T}_i^{field}$	torque of external magnetic field on particle i $(N.m)$		

5. References

[1] N. Sezer, M. A. Atieh, and M. Koç, "A comprehensive review on synthesis, stability, thermophysical properties, and characterization of nanofluids," *Powder technology,* vol. 344, pp. 404-431, 2019.

[2] B. M'hamed, N. A. C. Sidik, M. N. A. W. M. Yazid, R. Mamat, G. Najafi, and G. Kefayati, "A review on why researchers apply external magnetic field on nanofluids," *International Communications in Heat and Mass Transfer,* vol. 78, pp. 60-67, 2016.

[3] M. Yavari, Z. Mansourpour, and M. Shariaty-Niassar, "Controlled assembly and alignment of CNTs in ferrofluid: Application in tunable heat transfer," *Journal of Magnetism and Magnetic Materials,* vol. 479, pp. 170-178, 2019.

[4] I. Nkurikiyimfura, Y. Wang, and Z. Pan, "Effect of chain-like magnetite nanoparticle aggregates on thermal conductivity of magnetic nanofluid in magnetic field," *Experimental Thermal and Fluid Science,* vol. 44, pp. 607-612, 2013.

[5] A. Gavili, F. Zabihi, T. D. Isfahani, and J. Sabbaghzadeh, "The thermal conductivity of water base ferrofluids under magnetic field," *Experimental Thermal and Fluid Science,* vol. 41, pp. 94-98, 2012.

[6] O. M. Bunoiu, G. Matu, C. N. Marin, and I. Malaescu, "Investigation of some thermal parameters of ferrofluids in the presence of a static magnetic field," *Journal of Magnetism and Magnetic Materials,* vol. 498, p. 166132, 2020.

[7] S. Vinod and J. Philip, "Impact of field ramp rate on magnetic field assisted thermal transport in ferrofluids," *Journal of Molecular Liquids,* vol. 298, p. 112047, 2020.

[8] W. Liu, J. Alsarraf, A. Shahsavar, M. Rostamzadeh, M. Afrand, and T. K. Nguyen, "Impact of oscillating magnetic field on the thermal-conductivity of water-Fe3O4 and water-Fe3O4/CNT

Accepted Manuscript

ferro-fluids: Experimental study," *Journal of Magnetism and Magnetic Materials,* vol. 484, pp. 258-265, 2019.

[9] Z. Su, Y. Cheng, Z. Liu, J. Zhou, D. Li, and Y. Li, "Experimental Study on Thermal Conductivity of Water-Based Magnetic Fluid Loaded with Different Nanoparticles," *Nanomaterials,* vol. 13, no. 22, p. 2952, 2023.

[10] X.-h. Sun, M. Massoudi, N. Aubry, Z.-h. Chen, and W.-T. Wu, "Natural convection and anisotropic heat transfer in a ferro-nanofluid under magnetic field," *International Journal of Heat and Mass Transfer,* vol. 133, pp. 581-595, 2019.

[11] S. Mei, C. Qi, M. Liu, F. Fan, and L. Liang, "Effects of paralleled magnetic field on thermo-hydraulic performances of Fe3O4-water nanofluids in a circular tube," *International Journal of Heat and Mass Transfer,* vol. 134, pp. 707-721, 2019.

[12] T. Völker, E. Blums, and S. Odenbach, "Heat and mass transfer phenomena in magnetic fluids," *GAMM-Mitteilungen,* vol. 30, no. 1, pp. 185-194, 2007.

[13] H. Engler, A. Lange, D. Borin, and S. Odenbach, "Hindrance of thermomagnetic convection by the magnetoviscous effect," *International Journal of Heat and Mass Transfer,* vol. 60, pp. 499-504, 2013.

[14] M. Bahiraei and M. Hangi, "Flow and heat transfer characteristics of magnetic nanofluids: a review," *Journal of Magnetism and Magnetic Materials,* vol. 374, pp. 125-138, 2015.

[15] M. Goharkhah, A. Salarian, M. Ashjaee, and M. Shahabadi, "Convective heat transfer characteristics of magnetite nanofluid under the influence of constant and alternating magnetic field," *Powder Technology,* vol. 274, pp. 258-267, 2015.

[16] Z. Mansourpour, N. Mostoufi, and R. Sotudeh-Gharebagh, "Investigating agglomeration phenomena in an air-polyethylene fluidized bed using DEM–CFD approach," *Chemical Engineering Research and Design,* vol. 92, no. 1, pp. 102-118, 2014.

[17] B. Hoomans, J. Kuipers, W. J. Briels, and W. P. M. van Swaaij, "Discrete particle simulation of bubble and slug formation in a two-dimensional gas-fluidised bed: a hard-sphere approach," *Chemical Engineering Science,* vol. 51, no. 1, pp. 99-118, 1996.

[18] O. Golovnia, A. Popov, A. Sobolev, and G. Hadjipanayis, "Alignment of magnetic uniaxial particles in a magnetic field: Simulation," *Journal of magnetism and magnetic materials,* vol. 365, pp. 64-69, 2014.

[19] A. Katiyar, P. Dhar, T. Nandi, and S. K. Das, "Magnetic field induced augmented thermal conduction phenomenon in magneto-nanocolloids," *Journal of Magnetism and Magnetic Materials,* vol. 419, pp. 588-599, 2016.

[20] P. A. Cundall and O. D. Strack, "A discrete numerical model for granular assemblies," *geotechnique,* vol. 29, no. 1, pp. 47-65, 1979.

[21] R. Bird, "B., WE Stewart and EN Lightfoot,"," *Transport Phenomena", second edition, John Wiley & Sons, Inc,* 2002.

[22] X. Fang, Y. Xuan, and Q. Li, "Anisotropic thermal conductivity of magnetic fluids," *Progress in natural science,* vol. 19, no. 2, pp. 205-211, 2009.

[23] A. Satoh, *Introduction to practice of molecular simulation: molecular dynamics, Monte Carlo, Brownian dynamics, Lattice Boltzmann and dissipative particle dynamics*. Elsevier, 2010.

[24] H. Zhu, C. Zhang, S. Liu, Y. Tang, and Y. Yin, "Effects of nanoparticle clustering and alignment on thermal conductivities of Fe 3 O 4 aqueous nanofluids," *Applied Physics Letters,* vol. 89, no. 2, p. 023123, 2006.

[25] M. Abareshi, E. K. Goharshadi, S. M. Zebarjad, H. K. Fadafan, and A. Youssefi, "Fabrication, characterization and measurement of thermal conductivity of Fe3O4 nanofluids," *Journal of Magnetism and Magnetic Materials,* vol. 322, no. 24, pp. 3895-3901, 2010.

Accepted Manuscript

[26] P. Shima and J. Philip, "Tuning of thermal conductivity and rheology of nanofluids using an external stimulus," *The Journal of Physical Chemistry C,* vol. 115, no. 41, pp. 20097-20104, 2011.

[27] Q. Li, Y. Xuan, and J. Wang, "Experimental investigations on transport properties of magnetic fluids," *Experimental Thermal and Fluid Science,* vol. 30, no. 2, pp. 109-116, 2005.

[28] M. Ashjaee, M. Goharkhah, L. A. Khadem, and R. Ahmadi, "Effect of magnetic field on the forced convection heat transfer and pressure drop of a magnetic nanofluid in a miniature heat sink," *Heat and Mass Transfer,* vol. 51, pp. 953-964, 2015.

Accepted Manuscript